



Received: 22 February 2021

Revised: 23 March 2021

Accepted: 25 March 2021

# Mapping the electronic structure of polypyrrole with image-based electrochemical scanning tunneling spectroscopy

Roger Gonçalves<sup>1,2</sup> | Robert S. Paiva<sup>1</sup> | Andrés M. R. Ramírez<sup>2,3</sup> | Jonathan A. Mwanda<sup>2</sup> | Ernesto C. Pereira<sup>1</sup>  | Angel Cuesta<sup>2</sup> 

<sup>1</sup> Department of Chemistry, Federal University of São Carlos, São Carlos, Brazil

<sup>2</sup> Department of Chemistry, School of Natural and Computing Sciences, University of Aberdeen, Aberdeen, UK

<sup>3</sup> Department of Chemistry, Pontificia Universidad Católica de Chile, Santiago, Chile

## Correspondence

Angel Cuesta, Department of Chemistry, School of Natural and Computing Sciences, University of Aberdeen Aberdeen AB24 3UE, UK.  
 Email: [angel.cuestaciscar@abdn.ac.uk](mailto:angel.cuestaciscar@abdn.ac.uk)

## Abstract

Conducting polymers are semiconductors whose applications cover a wide range of devices. Their versatility is due, in addition to other factors, to properties that can be easily modulated according to the intended application. It is therefore important to study and map the electronic structure of these materials for a better correlation between structure and properties. Electrochemical scanning tunneling spectroscopy (EC-STs) can be a powerful tool to characterize the electronic structure of the semiconductor interface. In this work, we have used image-based EC-STs (IB-EC-STs) to describe quantitatively the band structure of an electrochemically deposited polypyrrole film. IB-EC-STs located the band edge of the polymer's valence band (VB) at 0.95 V vs. RHE (-5.33 eV in the absolute potential scale) and the intragap polaron states formed when the polymer is doped, at 0.46 V vs. RHE (-4.84 eV). The IB-EC-STs data were cross-checked with electrochemical impedance spectroscopy (EIS) and Mott-Schottky analysis of the interfacial capacitance. The DOS spectrum obtained from EIS data is consistent with the STS-deduced location of the VB and the polarons.

## KEYWORDS

electrochemical scanning tunneling microscopy, electronic structure, impedance spectroscopy, polypyrrole

## 1 | INTRODUCTION

Understanding the electronic structure of conducting polymers (CPs) is necessary for a detailed understanding of the behavior of these materials, whose mechanism of electronic conduction is different from that characteristic of inorganic semiconductors. It is therefore important to acquire the experimental information required to build

a complete model of their band structure, which governs their properties.<sup>1,2</sup>

Due to the size of CP molecules, atomic orbitals in the polymer chains combine to give rise to bands that extend throughout the entire macromolecule.<sup>3</sup> As in the case of inorganic semiconductors, the conductivity of the undoped material is associated with either free electrons in the conduction band (CB) or free holes in the valence

This is an open access article under the terms of the [Creative Commons Attribution](https://creativecommons.org/licenses/by/4.0/) License, which permits use, distribution and reproduction in any medium, provided the original work is properly cited.

© 2021 The Authors. *Electrochemical Science Advances* published by Wiley-VCH GmbH

band (VB) generated either by photo-excitation or (if the band gap is sufficiently small compared with  $kT$ ) by thermal excitation of electrons from the VB into the CB. In the case of inorganic semiconductors, the conductivity can be increased by injecting electrons or holes in either the CB or the VB through  $n$  or  $p$  doping, respectively, which typically results in the creation of an associated point defect in the material. On the other hand, doping of CPs is due to oxidation or reduction processes in the polymer, and does not result in the injection of electrons or holes in the CB or the VB, respectively, but in the formation of solitons, polarons, and, at high doping levels, bipolarons, localized within the energy gap.<sup>4,5</sup> In the particular case of  $p$ -doping a CP through oxidation, a radical cation (hole-polaron, spin 1/2) is created upon removal of an electron from the polymeric chain,<sup>5</sup> which could be understood as a rearrangement of  $\pi$  electrons that locally polarizes the polymer chain. In chemical terms, a polaron consists of a radical ion with unitary charge and a well-defined energy within the gap that can be detected, for example, via optical spectroscopy<sup>6</sup> (please note, however, that optical spectroscopy will provide the energy difference between the intragap level and the band edge, but never the exact location of the intragap level in a well-defined energy scale, unless the location of the band edge itself is also known). If a second electron is removed from the polymer chain, two situations can occur: (a) another hole-polaron state is created, or (b) if the polarons are close enough (*ie*, at high doping levels<sup>5,7</sup>) they collapse in a single, doubly charged defect, called bipolarons (spin 0).<sup>8–10</sup> In summary, like inorganic semiconductors, CPs can be doped in order to control their conductivity.<sup>11</sup> However, the charge carriers are not electrons or holes inside the CB and VB, respectively, but polarons and bipolarons located within the bandgap.<sup>12</sup>

Polypyrrole (PPy) is one of the most studied CPs because of its low oxidation potential, the water solubility of the monomer, and its low cost.<sup>13</sup> These unique properties make it compatible with devices working in aqueous media, in applications like drug delivery, biosensors, artificial muscles, and optoelectronic devices.<sup>14</sup> PPy was the first CP to be characterized by its optoelectronic properties, which can be altered by doping/de-doping.<sup>15</sup>

Scanning Tunneling Microscopy (STM) is a powerful technique based on the quantum tunneling effect that allows obtaining images of surfaces with atomic resolution.<sup>16</sup> When a sharp metallic tip is placed very close to a sample surface and a small bias voltage is applied, a tunneling current flows through the gap between them. This tunneling current can also flow through a liquid electrolyte, and it is measurable if the tip is properly isolated to decrease the magnitude of any faradaic currents below the level of the target tunneling current, enabling atomic resolution images of electrode surfaces.<sup>17,18</sup> The tunneling

current also depends strongly on the density of states, and tunneling current versus bias plots obtained during a fast scan (typically in the V/s region) of the tip-sample bias (*ie*, scanning tunneling spectroscopy, STS) have been used to elucidate the band structure of conducting polymers in ultra-high vacuum (UHV).<sup>19</sup> A problem with this approach, however, is that the energy levels obtained by UHV-based STS cannot be related to any useful energy scale, like the reversible hydrogen electrode (RHE) or the absolute potential scale. This could be solved by doing STS at the electrode-electrolyte interface (electrochemical STS, EC-STS), where the potential of both tip and sample can be referred to a common reference electrode, but this is particularly challenging, because, at the high scan rates needed to scan the tip potential, faradaic, and capacitive currents (which scale with the square root of and linearly with, respectively, the scan rate) easily obscure the tunneling current. A way around this problem is to use imaged-based EC-STS (IB-EC-STS), in which the tip potential versus a suitable reference electrode is scanned during imaging in either positive or negative direction until the STM image disappears, which must coincide with the moment at which a band edge is crossed and the Fermi level of the tip falls within the sample's band gap (where neither tunneling from the tip to the full VB nor from the empty CB to the tip is possible). This approach was used by Sanz and co-workers<sup>20</sup> to elucidate the band structure of the passive film on an iron electrode, and that work remains, to the best of our knowledge, the only example of IB-EC-STS

In this work, IB-EC-TS and energy-resolved electrochemical impedance spectroscopy (EIS) were combined to map the electronic structure of a PPy film and to obtain a quantitative description of its electronic structure.

## 2 | EXPERIMENTAL PROCEDURES

### 2.1 | Solutions and reactants

PPy was synthesized from pyrrole (Sigma-Aldrich) without further purification. For both electrosynthesis and electrochemical aqueous characterization, the electrolyte used was 0.1 mol/L HClO<sub>4</sub> (70%, Sigma-Aldrich) prepared using ultra-pure Milli-Q water (resistivity of 18.0 M $\Omega$  cm).

### 2.2 | Synthesis of Polypyrrole films

PPy films were synthesized electrochemically via cyclic voltammetry in a conventional three-electrode cell containing 0.1 mol/L HClO<sub>4</sub> + 0.1 mol/L pyrrole. The working

electrode was cycled 10 times at 50 mV/s in the potential range between 0.0 V and 1.0 V versus RHE. After the PPy growth, the substrate covered with the polymer film was rinsed with water and placed in an electrochemical cell containing pyrrole-free 0.1 mol/L HClO<sub>4</sub> for the measurements.

### 2.3 | Cyclic voltammetry and electrochemical impedance spectroscopy

Cyclic voltammetry and electrochemical impedance spectroscopy were performed using a conventional three-electrode configuration. The working electrode was either a Pt(111) single-crystal (prepared as described in Section 2.3) or a polycrystalline platinum electrode covered with PPy, with the substrate having no effect on the behaviour of the PPy film, and a Pt wire was used as counter electrode. A reversible hydrogen electrode (RHE) was used as reference. Cyclic voltammetry was carried out between 0.0 V and 1.0 V at a scan rate of 0.05 V/s, starting at 0.1 V in the positive direction to ensure that the PPy film was initially in the reduced (de-doped) state. The interfacial capacitance and the charge transfer resistance were determined at selected potentials by fitting the corresponding electrochemical impedance (EI) spectra to a transmission line model. EI spectra in the potential region between 0.0 V and 1.0 V were obtained by keeping the potential constant and superimposing an ac perturbation of 0.01 V, scanning the frequency between 10 kHz and 0.1 Hz.

### 2.4 | STM characterization

STM cells used were kept for at least 24 h in piranha solution (H<sub>2</sub>SO<sub>4</sub>/H<sub>2</sub>O<sub>2</sub>, 9:1) prior to use. They were then rinsed several times with ultra-pure water and boiled in ultra-pure water for half an hour, repeating the rinsing and boiling procedure at least 4 times. The Pt(111) electrode used for STM measurements was annealed in the flame of a Bunsen burner and then allowed to cool down to room temperature inside a flask containing a 3:1 N<sub>2</sub>:H<sub>2</sub> atmosphere.

Pt-Ir (80:20) tips were prepared by an electrochemical etching procedure,<sup>21–23</sup> a detailed description of which can be found in the Supplementary Information. Once etched, the tips were insulated using an electrophoretic paint in order to lower capacitive and faradaic currents down to a few pA or, at most, tens of pA. Details of the insulating procedure are provided below. STM images were recorded in the constant-current mode using a PicoLE Molecular Imaging with a PicoScan 2100 controller. Pt wires were used as counter and quasi reference electrodes.

## 3 | RESULTS AND DISCUSSION

### 3.1 | Electrochemical characterization

Figure 1A shows the cyclic voltammograms recorded during the growth of a PPy film on a Pt(111) electrode in a perchloric acid solution containing pyrrole. During growth, the current in the double-layer region increases linearly with increasing number of cycles (Figure 1A, inset), as expected. Considering the total charge involved in the deposition process (about 600 mC), a film several hundred nanometres in thickness was obtained. This ensures that tunneling occurs between the PPy film and tip, and not directly between the tip and the Pt(111) substrate.

After the 20<sup>th</sup> growth cycle, the voltammetric profile of the PPy film in a pyrrole-free perchloric acid solution agrees with those described in previous work for PPy in acidic media (Figure 1B).<sup>24–26</sup> The cyclic voltammogram is characterized by an oxidation process that starts around 0.12 V and peaks around 0.49 V, corresponding to the *p*-doping of the polymer. In addition, doping the obtained PPy film is quite reversible since the Coulombic efficiency (ratio of oxidation and reduction charges) was 93.6%.

Electrochemical impedance spectroscopy was used to obtain information about the electrochemical and electronic properties of the PPy film. The impedance results were fitted using a transmission line model<sup>24,27–31</sup>, which is presented in the Supporting Information (Part 2).

A plot of the inverse of the squared capacitance (Figure 2A), as obtained from the impedance measurements, can be used to determine the apparent charge-carrier density and the apparent flat-band potential by fitting the data to the Mott-Schottky equation:

$$\frac{1}{C^2} = \frac{2}{\epsilon_r \epsilon_0 e N_h} \left( E_{\text{fb}} - E + \frac{k_B T}{e} \right) \quad (1)$$

where  $\epsilon_r$  is the material's dielectric constant,  $\epsilon_0$  is the vacuum permittivity,  $e$  is the elementary charge,  $N_h$  is the density of majority charge carriers (in the PPy case, polaron and, at high doping levels, bipolaron holes),  $E_{\text{fb}}$  is the flat-band potential,  $E$  is the applied potential,  $k_B$  is the Boltzmann constant and  $T$  is the temperature in Kelvin. Figure 2A shows such a plot and fit, from where an apparent flat-band potential of 0.11 V and an apparent hole polaron density of  $3.31 \times 10^{19} \text{ cm}^{-3}$  is obtained. We will discuss these values later, in the light of the information obtained from the impedance-derived distribution of density of states (DOS) and the IB-EC-STs data.

The potential dependent charge transfer resistance ( $R_{\text{ct}}$ ), as obtained from EIS fitted data, can be used to calculate the DOS spectrum using the Gmucová-Nádaždy

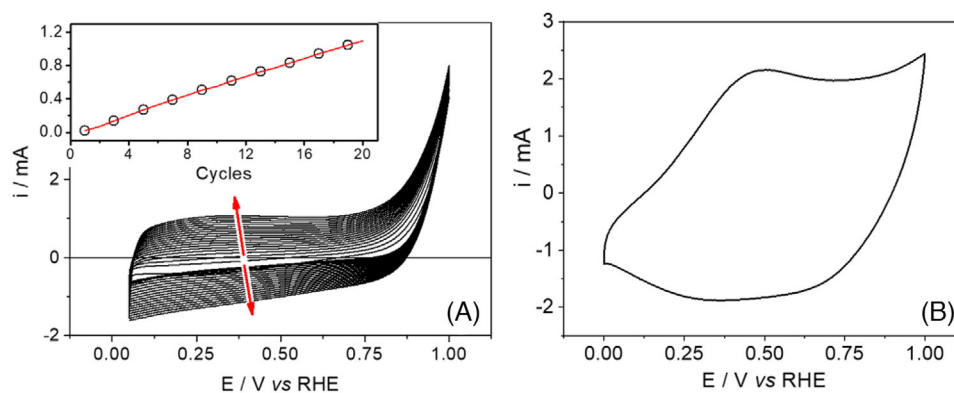


**FIGURE 1** (A) Cyclic voltammograms recorded during the growth of polypyrrole from 0.1 mol/L HClO<sub>4</sub> + 0.1 mol/L pyrrole solutions on a Pt(111) electrode. The inset shows the linear increase of the current at 0.04 V with increasing number of cycles; (B) cyclic voltammetry of PPy on Pt(111) in pyrrole-free 0.1 M HClO<sub>4</sub> mol/L. Scan rate: 0.05 V/s

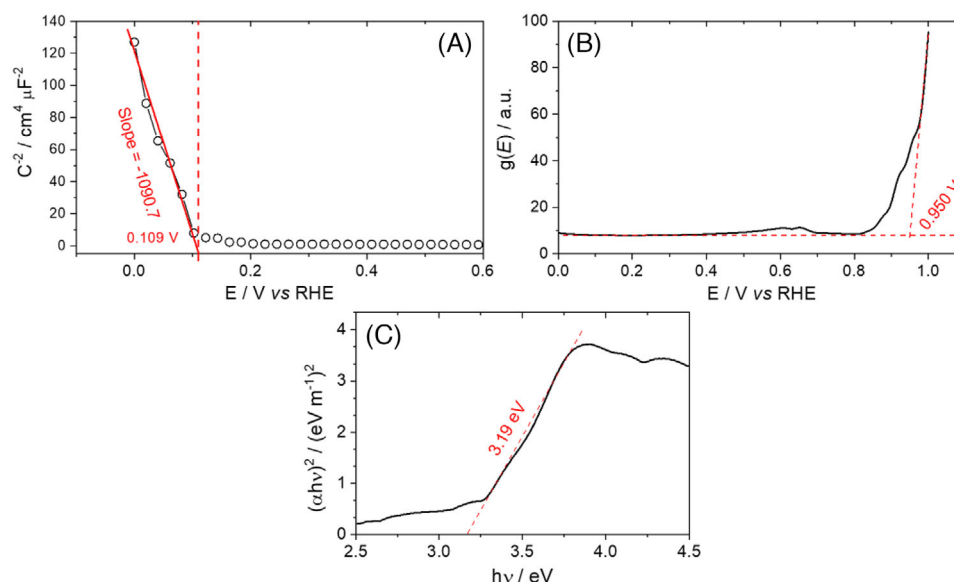


**FIGURE 2** Mott-Schottky plot (A), density of states (DOS) spectrum (B) and Tauc plot showing the determination of the (indirect) band gap energy from the optical absorption spectrum (C) of thin polypyrrole films grown on polycrystalline Pt after 20 voltammetric cycles.

equation<sup>32,33</sup>:

$$g(E_{fb,redox} = eU) = \frac{1}{ek_{et}[A]SR_{ct}} \quad (2)$$

where  $e$  is the elementary charge,  $k_{et}$ , is the charge-transfer constant in  $\text{cm}^4 \text{s}^{-1}$ ,  $[A]$  is the concentration in the electrolyte of redox (donor/acceptor) pairs in  $\text{cm}^{-3}$ ,  $S$  is the electrode area in  $\text{cm}^2$  and  $R_{ct}$  is the charge-transfer resistance in  $\Omega$ .

According to the authors, the technique allows, by means of electrochemical tests, to obtain the electrode density of states and in this way, to have an idea of bands or electronic states positions. Considering that the

electrode polarization slightly changes the state distribution in the electrode, it is not as accurate as other available techniques, however, on the other hand, by using only a potentiostat and a frequency response analyzer, this technique becomes quite promising. In addition, as most materials have wide bandgaps, added to the important need to reach the region where DOS presents a stable value, that is, indicating the maximum number of states and, therefore, the population present in the band itself, so that its edge was determined with greater precision, however, there is a need to scan the potential in solvents that allow a wide working window, such as acetonitrile.

However, after previous studies, it was noticed that PPy had a different voltammetric profile when in acetonitrile

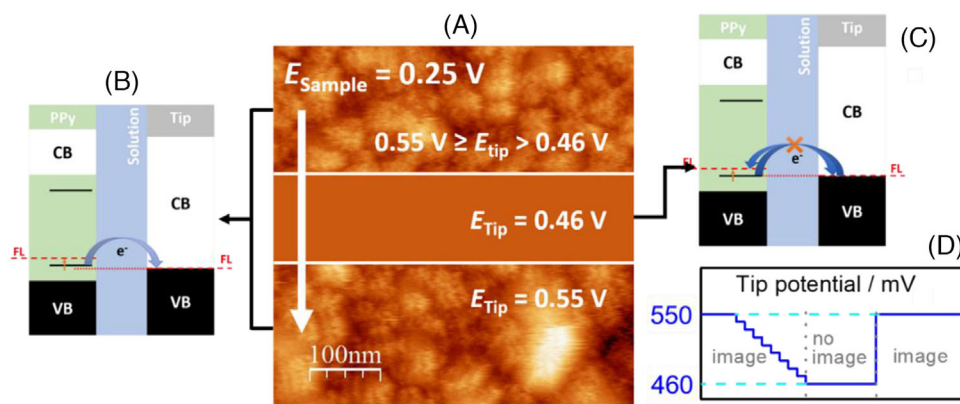


**FIGURE 3** (A) STM image ( $500 \times 500 \text{ nm}^2$ ) of a PPy film electrochemically grown on a Pt(111) electrode in 0.1 mol/L  $\text{HClO}_4$  at  $E_{\text{sample}} = 0.25 \text{ V}$ . The scan direction is from top to bottom, as indicated by the white arrow. Initially,  $E_{\text{tip}} = 0.55 \text{ V}$ .  $E_{\text{tip}}$  was then progressively made more negative in 0.01 V steps. The central region of the image was recorded at  $E_{\text{tip}} = 0.46 \text{ V}$ , and then  $E_{\text{tip}}$  was stepped back to the initial value of 0.55 V before recording the bottom part of the image; (B) Schematic representation of the location of the different energy levels when  $E_{\text{tip}} = 0.55 \text{ V}$ , with electrons tunneling from the intra-gap, half-filled, polaron hole state into the tip's Fermi level. The effect of band bending has been omitted for the sake of clarity and simplicity; (C) Schematic representation of the location of the different energy levels when  $E_{\text{tip}} \leq 0.46 \text{ V}$ . Tunneling is not possible either from the tip to the sample due to the positive tip bias, or from the sample to the tip, because there are no filled or partially filled electronic states above the tip's Fermi level. The effect of band bending has been omitted for the sake of clarity and simplicity; (D) Scheme illustrating the potential programme applied to the tip.  $I_T = 2 \text{ nA}$

and as the intention was to compare the value obtained through this technique with the IB-EC-STs data, it was decided to scan the potential in aqueous medium. On the other hand, this brought an important limitation: it was only possible to analyze the region of positive potential, corresponding to the edge of the PPy valence band. In addition, due to undesirable side reactions that could occur at potentials above 1.0 V RHE, it was not possible to go beyond this value. This potential limit did not allow visualizing the whole DOS value range, which is important to determine the bandwidth potential as the value of peak half-height. Thus, it was decided to extrapolate the ascending line of DOS values, Figure 2B shows the DOS spectrum of our PPy films, from which a location of the VB edge at 0.95 V could be estimated. This value will be compared below with that obtained from IB-EC-STs. Also useful for the analysis of IB-EC-STs data, the PPy bandgap was determined by UV-Vis-NIR diffuse reflectance spectroscopy and the Tauc plot was obtained using the Kubelka-Munk equation<sup>34</sup>, in which the value of  $n$  used was  $\frac{1}{2}$  (indirect bandgap). A value of 3.19 eV was estimated, consistent with the literature, whose values vary from 3.18 to 3.22 eV<sup>35–38</sup>.

### 3.2 | 4.2 Image-based electrochemical scanning tunneling spectroscopy

Figure 3 shows an STM image recorded at a sample potential  $E_{\text{sample}} = 0.25 \text{ V}$ , at which, according to the cyclic

voltammogram in Figure 1B, the PPy film must have been slightly oxidized (*ie*, some hole polarons must have been created), and an initial tip potential  $E_{\text{Tip}} = 0.55 \text{ V}$ . Under these conditions, imaging should be impossible, because electrons should tunnel from the sample (more negative potential, equivalently, higher  $E_F$ ) to the tip (more positive potential, equivalently, lower  $E_F$ ) but, according to the DOS spectrum in Figure 2B, the  $E_F$  of the tip lies exactly within the PPy's band gap and there are no occupied states from which this could happen.

A clear image can however be obtained (Figure 3A), which can only be explained if a half-filled polaron level is located at an energy higher than the tip's  $E_F$ . In order to test this hypothesis, the tip potential was slowly scanned in the negative direction, which results in the image disappearing at 0.46 V (Figure 3A). The disappearance of the image is accompanied by a saturation of the piezo in the Z-direction, which indicates that the feedback circuit has forced the tip to move towards the sample to the maximum extent allowed by the traveling distance of the piezo tube in the Z-direction. Because the thickness of the PPy film is several hundreds of nanometres and the total traveling distance of our piezo tube in the Z-direction is 1  $\mu\text{m}$ , the piezo saturates before the tip can approach the Pt substrate close enough for tunneling to occur directly to/from Pt to the tip (please note that the starting point is usually half-way thorough the total traveling length of the Z-piezo, in order to allow maximum flexibility for the tip to adapt its position to both increases and decreases in the tunneling current during imaging) This results in a featureless image. The usual

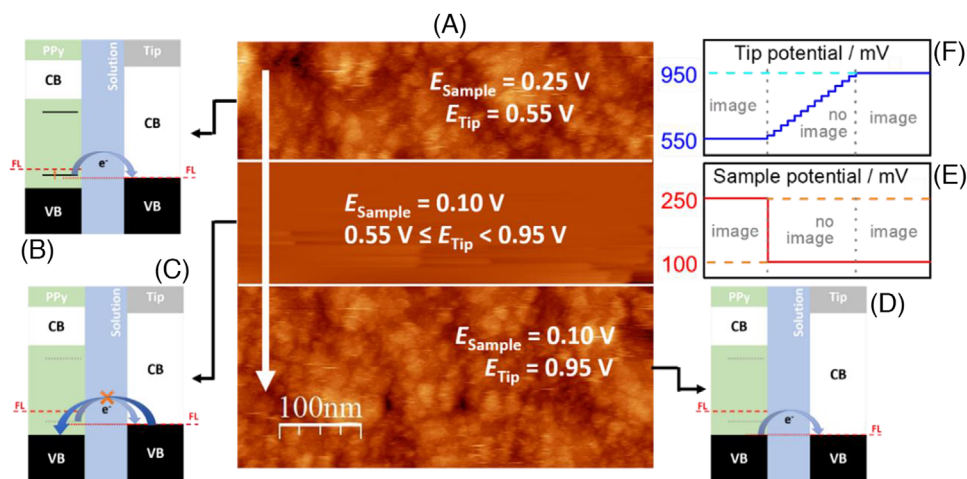


**FIGURE 4** (A) STM image ( $500 \times 500 \text{ nm}^2$ ) of a PPy film electrochemically grown on a Pt(111) electrode in 0.1 mol/L  $\text{HClO}_4$  at initial  $E_{\text{sample}} = 0.25 \text{ V}$  and  $E_{\text{tip}} = 0.55 \text{ V}$ . The scan direction is from top to bottom, as indicated by the white arrow.  $E_{\text{sample}}$  was stepped to 0.10 V approximately one quarter down the image. The central region of the image was recorded at  $E_{\text{sample}} = 0.10 \text{ V}$  while  $E_{\text{tip}}$  was increased from 0.55 to 0.95 V in 0.01 V steps. The bottom section of the image was recorded at  $E_{\text{sample}} = 0.10 \text{ V}$  and  $E_{\text{tip}} = 0.95 \text{ V}$ ; (B) Schematic representation of the location of the different energy levels when  $E_{\text{tip}} = 0.55 \text{ V}$  and  $E_{\text{sample}} = 0.25 \text{ V}$ , with electrons tunnelling from the intra-gap, half-filled, polaron hole state into the tip's Fermi level. The effect of band bending has been omitted for the sake of clarity and simplicity; (C) Schematic representation of the location of the different energy levels when  $E_{\text{sample}} = 0.10 \text{ V}$  and  $0.55 \text{ V} \leq E_{\text{tip}} < 0.95 \text{ V}$ . Tunnelling is not possible either from the tip to the sample due to the positive tip bias or from the sample to the tip, because there are no filled or partially filled electronic states above the tip's Fermi level. The effect of band bending has been omitted for the sake of clarity and simplicity; (D) Schematic representation of the location of the different energy levels when  $E_{\text{sample}} = 0.10 \text{ V}$  and  $E_{\text{tip}} = 0.95 \text{ V}$ . Tunnelling is now possible from PPy's VB into the tip's Fermi level; (E) and (F) Schemes illustrating the potential programs applied to sample and tip, respectively.  $I_T = 2 \text{ nA}$

line-by-line background subtraction performed to correct for the slight inclination of the sample is the reason why the image does not appear dark. The image reappears if the tip potential is then stepped back to 0.55 V, as shown in the lower part of the image (Figure 3A). This allows us to locate the position of the hole polaron at 0.46 V vs. RHE, which is in good agreement with the small DOS between 0.4 and 0.7 V in the DOS spectrum in Figure 2B. The behavior observed in Figure 3 can be explained as follows: when  $E_{\text{tip}} \leq 0.46 \text{ V}$  but more positive than the sample potential (0.25 V), the flow of electrons from the sample to the tip (as dictated by the positive tip bias) is not possible because the VB edge is lower in energy than the tip's Fermi level, and the electronic states in the CB are all empty at room temperature (Figure 3C). On the contrary, when  $E_{\text{tip}} > 0.46 \text{ V}$ , the tip's energy level lies at a lower level than the half-filled polaron hole, which allows electrons to tunnel from the latter into the tip and an STM image to be established (Figure 3B).

The experiment shown in Figure 4 confirms that imaging in the top and bottom sections of Figure 3A was due to tunneling from intra-gap, half-filled polaron states. As in Figure 3,  $E_{\text{tip}}$  and  $E_{\text{sample}}$  were initially set at 0.55 and 0.25 V, respectively. A clear image was obtained under these conditions, reproducing the results in Figure 3A. Instead of changing  $E_{\text{tip}}$ , as in Figure 3, in this experiment  $E_{\text{tip}}$  was kept constant and  $E_{\text{sample}}$  was stepped to

0.10 V after having scanned approximately  $\frac{1}{4}$  of the image area (Figure 4A). According to the cyclic voltammogram in Figure 1B, at 0.1 V the oxidized polymer units should be reduced, in other words, this potential step should result in the de-doping of PPy and the disappearance of the half-filled polaron states. As expected, the image vanishes after the potential step (Figure 4A), confirming that imaging was due to tunneling from the hole polaron states (see Figures 4B,C).  $E_{\text{tip}}$  was then slowly made more positive until the image reappeared at  $E_{\text{tip}} = 0.95 \text{ V}$  (Figure 4A). This must correspond to the potential at which the Fermi level of the tip crosses the VB edge, allowing the tip to receive electrons from the VB (Figure 4D). This is in good agreement with the location of the VB edge as obtained from the EIS-derived DOS spectrum.

Because hole polaron levels are half-filled, tunneling from the tip to these levels must be possible under negative tip bias. This is confirmed by the results in Figure 5. In this case,  $E_{\text{sample}}$  was set at 0.25 V and  $E_{\text{tip}}$  was initially set at 0.49 V. As we have seen above, polaron states have already been created at this  $E_{\text{sample}}$ , and tunneling from these to the tip results in a clear STM image (Figures 5A and B).  $E_{\text{tip}}$  was then slowly scanned in the negative direction in 0.01 V steps, until the polaron level is crossed at 0.43 V (please note that a Pt wire was used as quasi-reference in these spectra, which accounts for the small difference in the location of the polaron level in Figures 3 and 5), at which

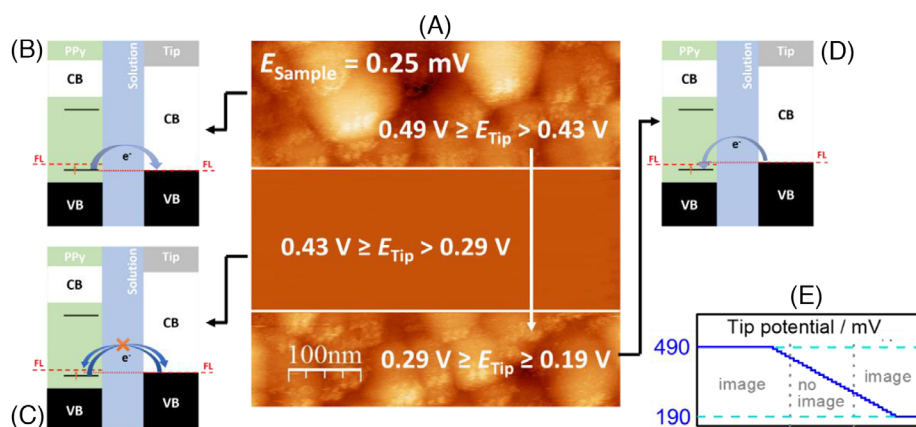


**FIGURE 5** (A) STM image ( $500 \times 500 \text{ nm}^2$ ) of a PPy film electrochemically grown on a Pt(111) electrode in 0.1 mol/L  $\text{HClO}_4$  at  $E_{\text{sample}} = 0.25 \text{ V}$ . The scan direction is from top to bottom, as indicated by the white arrow. Initially,  $E_{\text{tip}} = 0.49 \text{ V}$ , and was then progressively made more negative in 0.01 V steps. The central region of the image was recorded at  $E_{\text{tip}}$  between 0.43 and 0.29 V, and the bottom section of the image at  $E_{\text{tip}}$  between 0.29 and 0.19 V; (B) Schematic representation of the location of the different energy levels when  $E_{\text{tip}} > 0.43 \text{ V}$ , with electrons tunneling from the intra-gap, half-filled, polaron hole state into the tip's Fermi level. The effect of band bending has been omitted for the sake of clarity and simplicity; (C) Schematic representation of the location of the different energy levels when  $E_{\text{tip}}$  is between 0.43 and 0.29 V. Tunnelling is not possible either from the tip to the sample, due to the positive tip bias, or from the sample to the tip, because there are no filled or partially filled electronic states above the tip's Fermi level; (D) Schematic representation of the location of the different energy levels when  $E_{\text{tip}}$  between 0.29 and 0.19 V. Tunneling is now possible from the tip to the sample due to the negative tip bias and the presence of partially filled polaron levels below the tip's Fermi level. The effect of band bending has been omitted for the sake of clarity and simplicity; (E) Scheme illustrating the potential program applied to the tip.  $I_T = 2 \text{ nA}$ . In schematics (B, C, D), the effect of band bending has been omitted for the sake of clarity and simplicity

the image disappears for the reasons explained above (Figures 5A and C). However, when the  $E_{\text{tip}}$  reaches a value of 0.29 V and the tip crosses the sample's Fermi level, the STM image is recovered because now electrons can tunnel from the tip to the half-filled polaron level (Figures 5A,D). (Please note that tunneling from a more positive tip at 0.29 V to a more negative sample at 0.25 V should not be possible. However, due to an instrumental offset between the zeroes of the tip and sample potential scales, the actual and nominal bias do not coincide exactly, which, among other things, allows imaging when the nominal bias is zero and adds to the error in the determination of the energy levels.)

Our IB-EC-STs results allow us to build a quantitative energy diagram for PPy (Figure 6). For the absolute potential scale, a value of -4.44 eV for the absolute potential of the SHE was used, as recommended by Trasatti<sup>39</sup>, which sets the absolute potential of the RHE at pH 1 at -4.38 eV. The diagram is consistent with others reported in the literature obtained by spectroscopic methods.<sup>1,15,35</sup>

We would like to finish with a brief comment regarding the value of the flat-band potential as obtained from a Mott-Schottky analysis of the interfacial capacitance. The applicability and pitfalls of Mott-Schottky analysis and other methods for the determination of flat-band potentials have recently been discussed by Hankin et al.<sup>40</sup> As discussed by them, Mott Schottky analysis rests on

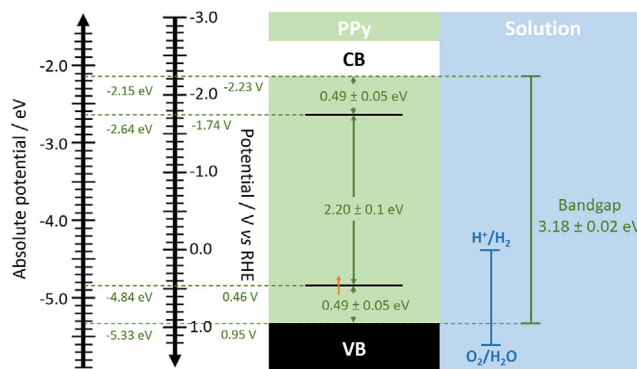


**FIGURE 6** Band diagram of a thin polypyrrole film on Pt as deduced from image-based electrochemical scanning tunneling spectroscopy in 0.1 mol/L  $\text{HClO}_4$ . The energy levels are indicated in both the RHE and the absolute potential scales

the assumption that the capacitance of the interface is dominated by that of the semiconductor's space-charge region or that, equivalently, the potential drop across the electrolyte side of the interface is much smaller than that across the space-charge region, which might not always be the case and would limit the applicability of the Mott-Schottky equation. We would like to add here that, for materials like PPy for which the doping level is continuously increasing with increasing potential (other materials like hydrogen tungsten bronzes, whose

conductivity depends on the W(V)/W(VI) ratio, could also fall in this category), the flat-band potential must also be continuously changing, which will further limit Mott-Schottky's applicability. In our particular example, we would expect the flat-band potential of undoped PPy to lie close, if not exactly at, the center of the gap, that is, around -0.64 V versus RHE. On the contrary, Mott-Schottky delivers a much more positive value of the apparent flat-band potential of *ca.* 0.11 V versus RHE, only 0.35 eV higher than the polaron level. The location of the flat band potential will be dragged down in energy as partially filled states are created some hundreds of mV above the band edge, and the apparent flat-band potential might therefore correspond instead to that of doped PPy, but the question is then what level of doping leads to this value. Alternatively, the apparent flat-band potential might indicate the onset potential of PPy oxidation (*i.e.*, of PPy doping) which would agree with the cyclic voltammogram (Figure 1B) and the observation in Figure 4 that tunnelling from the sample to the tip is not possible when  $E_{\text{sample}} \leq 0.1$  V and  $E_{\text{tip}}$  is more positive than  $E_{\text{sample}}$  but more negative than 0.95 V (the valence band edge). More research is probably needed to solve this question.

## 4 | CONCLUSION

IB-EC-STs was demonstrated as a tool that allows to achieve a complete characterization of the band structure of a PPy film on Pt, which was consistent with the DOS spectrum obtained from electrochemical impedance spectroscopy. The advantage of IB-EC-STs over other methods is that the information regarding the electronic levels is obtained directly and does not rely on the application of a model.


## ACKNOWLEDGMENTS

The support of this research by FAPESP (grants: 2013/07296-2, 2014/50249-8, 2015/12851-0, 2017/11986-5), Shell, CsF-PVE (99999.007708/2015-07), Coordenação de Aperfeiçoamento de Pessoal de Nível Superior - Brasil (CAPES) - Finance Code 001 and CNPq is gratefully acknowledged.

## DATA AVAILABILITY STATEMENT

The data that support the findings of this study are available from the corresponding author upon reasonable request.

## ORCID

Ernesto C. Pereira  <https://orcid.org/0000-0003-1058-302X>

Angel Cuesta  <https://orcid.org/0000-0003-4243-1848>

## REFERENCES

- W. H. Smyrl, M. Lien, in *Appl. Electroact. Polym.*, Springer Netherlands, Dordrecht, **1993**, pp. 29–74.
- R. J. Waltman, J. Bargon, P. Chemie, U. Bonn, W. Germany, R. J. Waltman, J. Bargon, *Can. J. Chem.* **1986**, *64*, 76–95.
- P. Y. Yu, M. Cardona, in *Fundam. Semicond.*, **2010**, pp. 17–106.
- P. Y. Yu, M. Cardona, in *Fundam. Semicond.*, **2010**, pp. 203–241.
- J. L. Bredas, G. B. Street, *Acc. Chem. Res.* **1985**, *18*, 309–315.
- A. R. Nagaraja, N. H. Perry, T. O. Mason, Y. Tang, M. Grayson, T. R. Paudel, S. Lany, A. Zunger, *J. Am. Ceram. Soc.* **2012**, *95*, 269–274.
- A. O. Patil, A. J. Heeger, F. Wudl, *Chem. Rev.* **1988**, *88*, 183–200.
- I. Sakellis, A. N. Papathanassiou, J. Grammatikakis, *Appl. Phys. Lett.* **2008**, *92*, 222108.
- G. Paasch, S. Scheinert, A. Petr, L. Dunsch, *Russ. J. Electrochem.* **2006**, *42*, 1161–1168.
- M. S. Sercheli, L. O. S. Bulho, **2000**, *631*, 631–634.
- H. E. Toma, *Química Nov. na Esc.* **1997**, 8–12.
- R. Faez, C. Reis, P. FREITAS, O. Kosima, *Química Nov. na Esc.* **2000**, 13–18.
- L.-X. Wang, X.-G. Li, Y.-L. Yang, *React. Funct. Polym.* **2001**, *47*, 125–139.
- Z.-B. Huang, G.-F. Yin, X.-M. Liao, J.-W. Gu, *Front. Mater. Sci.* **2014**, *8*, 39–45.
- E. M. Genies, G. Bidan, A. F. Diaz, *J. Electroanal. Chem.* **1983**, *149*, 101–113.
- K. Gentz, K. Wandelt, *Chim. Int. J. Chem.* **2012**, *66*, 44–51.
- H. J. W. Zandvliet, A. van Houselt, *Annu. Rev. Anal. Chem.* **2009**, *2*, 37–55.
- A. K. Yagati, J. Min, J.-W. Choi, in *Mod. Electrochem. Methods Nano, Surf. Corros. Sci.*, InTech, **2014**.
- S. Wakabayashi, H. Kato, M. Tomitori, O. Nishikawa, *J. Appl. Phys.* **1994**, *76*, 5595–5597.
- I. Diéz-Pérez, P. Gorostiza, F. Sanz, *J. Electrochem. Soc.* **2003**, *150*, B348.
- R. García, *Surf. Sci. Rep.* **2002**, *47*, 197–301.
- Z. Q. Yu, C. M. Wang, Y. Du, S. Thevuthasan, I. Lyubinetzky, *Ultramicroscopy* **2008**, *108*, 873–877.
- F. P. Zamborini, R. M. Crooks, *Langmuir* **1997**, *13*, 122–126.
- G. Garcia-Belmonte, J. Bisquert, *Electrochim. Acta* **2002**, *47*, 4263–4272.
- J. Bisquert, G. G. Belmonte, F. F. Santiago, N. S. Ferriols, M. Yamashita, E. C. Pereira, *Electrochem. commun.* **2000**, *2*, 601–605.
- T. F. Otero, *Polym. Rev.* **2013**, *53*, 311–351.
- G. Paasch, *Synth. Met.* **2001**, *119*, 233–234.
- G. Paasch, *Electrochim. Acta* **2002**, *47*, 2049–2053.
- J. Bisquert, A. Compte, *J. Electroanal. Chem.* **2001**, *499*, 112–120.
- R. Gonçalves, A. A. A. Correa, R. Pereira, E. C. C. Pereira, *Electrochim. Acta* **2016**, *190*, 329–336.
- A. A. Correa, R. Gonçalves, R. Pereira, E. C. Pereira, *J. Appl. Polym. Sci.* **2017**, *134*, DOI 10.1002/app.44368.
- K. Gmucová, V. Nádaždy, F. Schauer, M. Kaiser, E. Majková, *J. Phys. Chem. C* **2015**, *119*, 15926–15934.
- V. Nádaždy, F. Schauer, K. Gmucová, *Appl. Phys. Lett.* **2014**, *105*, 142109.



34. A. B. Murphy, *Sol. Energy Mater. Sol. Cells* **2007**, *91*, 1326–1337.
35. M. J. L. J. L. Santos, A. G. G. Brolo, E. M. M. Girotto, *Electrochim. Acta* **2007**, *52*, 6141–6145.
36. M. M. Abdi, H. N. M. Ekramul Mahmud, L. C. Abdullah, A. Kasim, M. Zaki Ab. Rahman, J. L. Y. Chyi, *Chinese J. Polym. Sci.* **2012**, *30*, 93–100.
37. V. Figá, Z. Essaidi, *J. Optoelectron. Adv. Mater.* **2008**, *10*, 3392–3397.
38. A. L. Botelho, Y. Shin, J. Liu, X. Lin, *PLoS One* **2014**, *9*, e86370.
39. S. Trasatti, *J. Electroanal. Chem. Interfacial Electrochem.* **1986**, *209*, 417–428.
40. A. Hankin, F. E. Bedoya-Lora, J. C. Alexander, A. Regoutz, G. H. Kelsall, *J. Mater. Chem. A* **2019**, *7*, 26162–26176.

## SUPPORTING INFORMATION

Additional supporting information may be found online in the Supporting Information section at the end of the article.

**How to cite this article:** R. Gonçalves, R. S. Paiva, A. M. R. Ramírez, J. A. Mwanda, E. C. Pereira, A. Cuesta. *Electrochem Sci Adv.* 2021, e2100028. <https://doi.org/10.1002/elsa.202100028>